

THE STRUCTURAL EVOLUTION OF FORMING AND EARLY STAGE STAR CLUSTERS

KARL O. JAEHNIG¹, NICOLA DA RIO¹, JONATHAN C. TAN^{1,2}¹Department of Astronomy, University of Florida, Gainesville, FL 32611, USA.²Department of Physics, University of Florida, Gainesville, FL 32611, USA.

ABSTRACT

We study the degree of angular substructure in the stellar position distribution of young members of Galactic star-forming regions, looking for correlations with distance from cluster center, surface number density of stars, and local dynamical age. To this end we adopt the catalog of members in 18 young ($\sim 1\text{--}3$ Myr) clusters from the *Massive Young Star-Forming Complex Study in Infrared and X-ray* (MYStIX) Survey and the statistical analysis of the Angular Dispersion Parameter, $\delta_{\text{ADP},N}$. We find statistically significant correlation between $\delta_{\text{ADP},N}$ and physical projected distance from the center of the clusters, with the centers appearing smoother than the outskirts, consistent with more rapid dynamical processing on local dynamical, free-fall or orbital timescales. Similarly, smoother distributions are seen in regions of higher surface density, or older dynamical ages. These results indicate that dynamical processing that erases substructure is already well-advanced in young, sometimes still-forming, clusters. Such observations of the dissipation of substructure have the potential to constrain theoretical models of the dynamical evolution of young and forming clusters.

Subject headings: stars: formation; stars: kinematics and dynamics; open clusters and associations: general

1. INTRODUCTION

It is well known that the majority of stars form in aggregates or clusters (Lada & Lada 2003; Gutermuth et al. 2009), which often do not survive as bound systems after early dynamical evolution and/or gas removal. As star formation progresses from early, more filamentary structures (e.g., André et al. 2013) to young clusters or field stars, understanding the evolution of the spatial and kinematic structures of star-forming regions can provide fundamental clues on the boundary conditions of the star formation process.

Numerical simulations suggest that virialized star clusters can form before gas expulsion (e.g., Fellhauer et al. 2009), depending on the initial conditions and time of gas removal. Subvirial initial conditions for stellar motions are also a possibility, as suggested by studies of dense gas cores (e.g., Kirk et al. 2007), with subsequent dynamical evolution investigated by a number of works (e.g., Scally & Clarke 2002; Proszkow & Adams 2009; Allison et al. 2009; Maschberger et al. 2010; Parker & Meyer 2012; Kruijssen et al. 2012).

Different studies have adopted several metrics to measure substructure (e.g., Goodwin & Whitworth 2004; Cartwright & Whitworth 2004; Gutermuth et al. 2005; Schmeja & Klessen 2006), e.g., the minimum spanning tree \mathcal{Q} parameter, mass surface density, stellar separation, and indicators of mass segregation. Parker et al. (2014); Parker (2014) showed that the use of multiple indicators at once helps disentangle effects of dynamical evolution from effects related to the choice of initial conditions.

In Da Rio et al. (2014) (hereafter DTJ14) we presented an analysis of the spatial distribution (as well as dynamical status) of sources in the Orion Nebula Cluster (ONC). We introduced a metric to measure the degree of angular subclustering in centrally concentrated clusters: *the*

angular dispersion parameter ($\delta_{\text{ADP},N}$), building on previous work by Gutermuth et al. (2005). This quantity represents the dispersion of stellar counts measured in N equal sectors from the cluster center, normalized to the standard deviation expected from Poisson statistics. Thus, $\delta_{\text{ADP},N} \simeq 1$ for an azimuthally random distribution, and increases in the presence of substructure. In contrast to other popular indicators of substructure, e.g., the minimum spanning tree \mathcal{Q} parameter (Cartwright & Whitworth 2004), $\delta_{\text{ADP},N}$ is sensitive to minute deviations from isotropy within a clearly defined stellar grouping, rather than only distinguishing among centrally concentrated versus substructured populations. In the ONC we detect a clear radial dependence of $\delta_{\text{ADP},N}$, with the core being systematically smoother than the outskirts, which we interpret as result of dynamical processing.

In this paper we extend this analysis to a sample of 18 clusters, including the ONC, from the MYStIX Survey (Feigelson et al. 2013). §2 is an overview of the data used for the analysis. Section §3 reviews our methods to calculate the center and the $\delta_{\text{ADP},N}$ radial variation for each cluster. We outline our findings in §4.

2. THE DATA

We adopt the dataset from the MYStIX survey (Feigelson et al. 2013). This survey collected data from the *Chandra* X-ray Observatory, and infrared photometry from the *United Kingdom InfraRed Telescope* (UKIRT) and the *Spitzer Space Telescope* on 20 Galactic star-forming regions with typical ages of 1–3 Myr (Getman et al. 2014b). From all the these sources, Broos et al. (2013) published statistical memberships based on multiple observational information: X-ray classification and infrared excess from circumstellar material. We thus restricted our analysis to these sources, for a total of 31,784 probable PMS stars. Due to sensitivity limits and the restrictive criteria of membership assignment, the MYStIX sample is incomplete especially for low-mass stars. How-

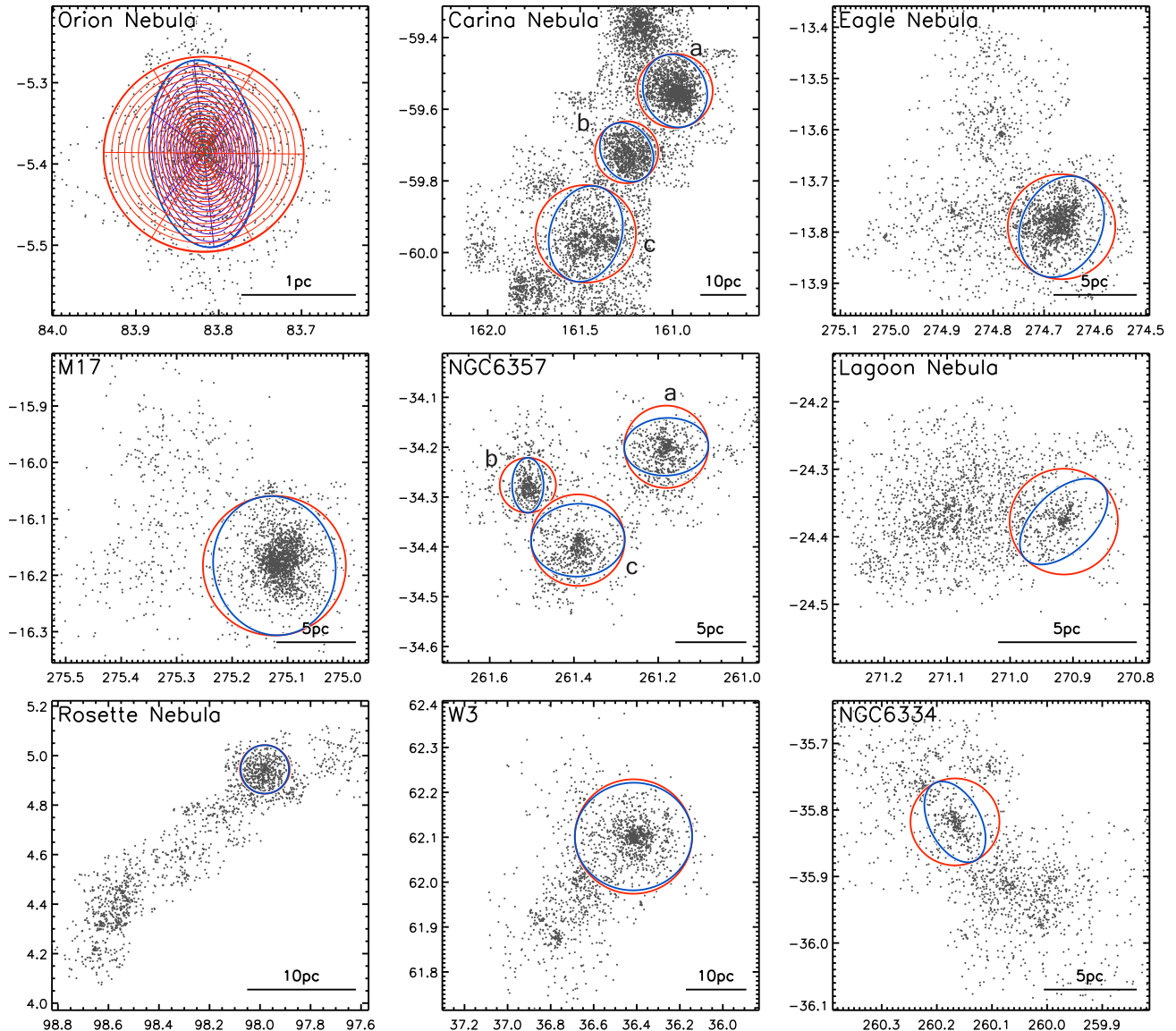


FIG. 1.— Spatial distribution of young candidate members in the considered MYStIX star-forming regions. The red circles indicate the outer cluster radius for each identified subcluster; the blue ellipses represent the best-fit 2D Plummer ellipsoid adopted to remove the contribution from the elongation of these structures in the $\delta_{\text{ADP},N}$ analysis. The physical distances indicated are computed adopting the cluster distances from Feigelson et al. (2013). In the first panel we illustrate the subdivision of the Orion population in concentric annuli containing 60 stars each (20 annuli for circular symmetry (red), 17 for elliptical symmetry (blue)). — *Continues on Figure 2.*

ever, we assume that the sample is representative of the spatial distribution of sources in each region. We exclude from our analysis two MYStIX clusters: the Trifid Nebula and W4, which respectively are characterized by low number statistics, or lack a definite central concentration, two aspects which undermine the diagnostic power of $\delta_{\text{ADP},N}$.

Some of the regions enclose multiple separated star clusters; Kuhn et al. (2014) identify MYStIX subclusters using collections of isothermal ellipsoids. We do not use their identification of subclusters since some of these groupings are poorly populated, unsuitable for $\delta_{\text{ADP},N}$ analysis, and in many cases they indicate a stratification or core-halo distribution which could simply indicate that these systems are not well fit by a single isothermal ellipsoid. Instead, we look for clusters using a nearest neighbor algorithm identifying overdensities at a scale of 0.065 pc. We isolate 22 subclusters in 18 star-forming

regions, as shown in Figures 1 and 2. For each cluster, we defined an outer boundary radius to be fully contained inside each Chandra field of view, and decreased it in some cases to avoid including multiple subclusters within the same aperture.

3. ANALYSIS

For each subcluster we refined the determination of the center using an iterative method, as in DTJ14: we start from the maximum of the nearest neighbor map, and recompute the center of stellar positions recursively while decreasing the aperture size for this computation until a convergence is found.

For a full description of the Angular Dispersion Parameter $\delta_{\text{ADP},N}$ we refer the reader to DTJ14; here we summarize its definition and characteristics. Given a circular (or elliptical) aperture, or one of some concentric annuli enclosed in it, the area is divided in N sectors

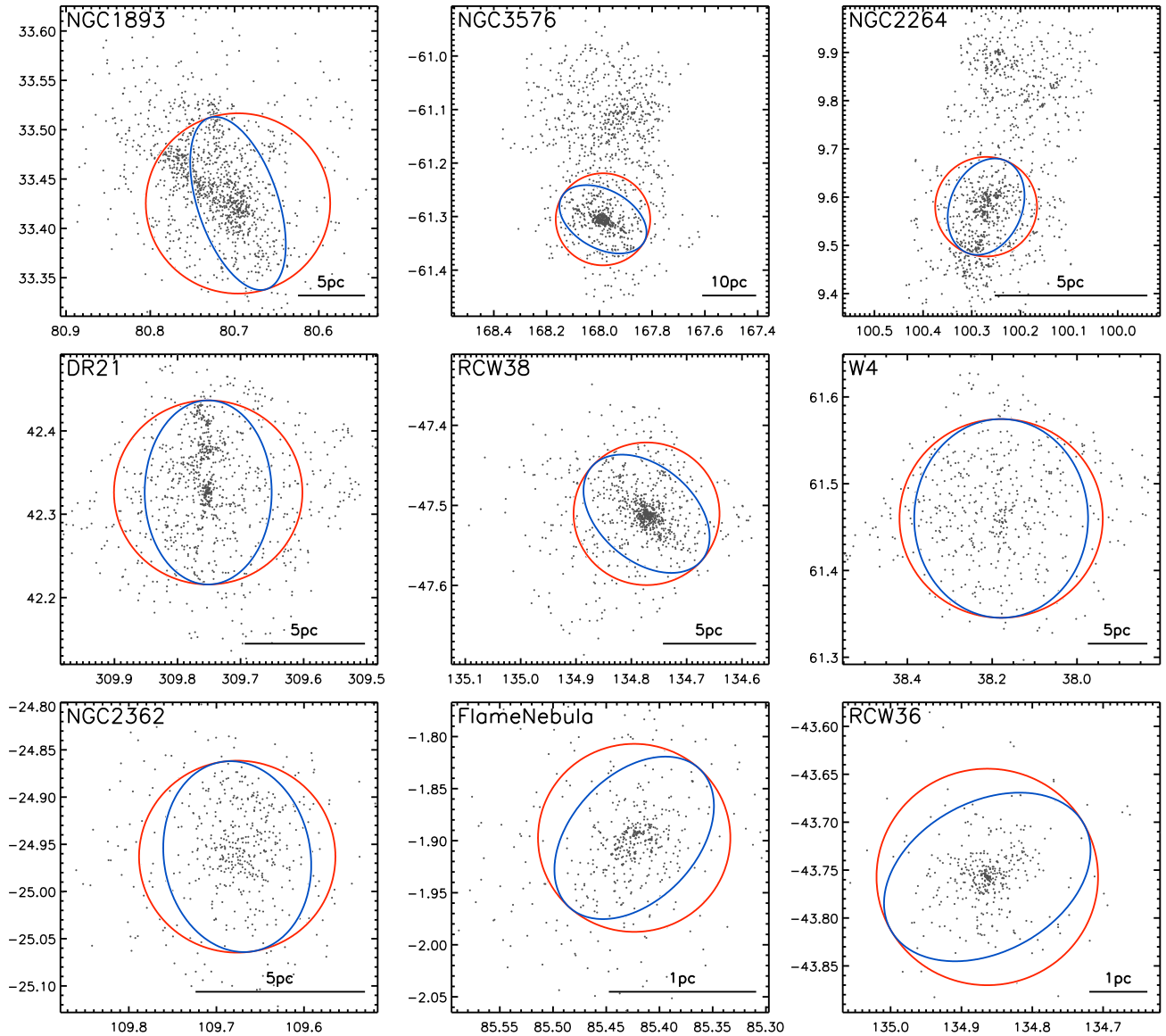


FIG. 2.— Continued from Figure 1.

of equal area, each containing n_i stars. $\delta_{\text{ADP},N}$ is then computed as:

$$\delta_{\text{ADP},N} = \sqrt{\frac{1}{(N-1)\bar{n}} \sum_{i=1}^N (n_i - \bar{n})^2} = \sqrt{\frac{\sigma^2}{\sigma_{\text{Poisson}}^2}}. \quad (1)$$

This parameter is subject to a statistical error, which does not depend only on the number of sectors N , and can be decreased further by averaging all possible orientations of the sector pattern (see DTJ14). For an isotropic centrally concentrated cluster, $\delta_{\text{ADP},N} \simeq 1$. Given a substructured morphology the actual value of $\delta_{\text{ADP},N} > 1$ depends on the number of stars in each annular region, which therefore must be fixed for a meaningful comparison between regions. We choose 60 stars per annulus as a compromise between statistical significance of number counts, and radial resolution. An example of the subdivision of the ONC population in circular or elliptical annuli is shown in the first panel of Figure 1. Depending on N , $\delta_{\text{ADP},N}$ measures a given angular mode

of substructure. As default for our analysis we consider $N = 6$, but also test the effect in our results assuming $N = 4$ or 9 .

As shown in DTJ14, ellipticity causes $\delta_{\text{ADP},N}$ to increase even for a smooth distribution, mimicking the effect of substructure, and, e.g., was found to be a main contributor to the measured $\delta_{\text{ADP},N} > 1$. This is because at a given distance (in circular symmetry) from the center the number counts are higher along the major axis and lower along the minor axis. A similar bias was also shown to affect the MST \mathcal{Q} parameter (Bastian et al. 2009). Thus in DTJ14 we generalized the $\delta_{\text{ADP},N}$ method to measure subclustering adopting elliptical symmetry – i.e., dividing the population into elliptical concentric sectors. For the sample here, we thus determined elongation by fitting simple 2D Plummer models to each cluster, leaving ellipticity and semi-major axis position angles as free parameters. In Figures 1 and 2 we display the 18 MYStiX regions, highlighting the subclusters selected for this study. The red circles denote the maximum useful apertures (R_{max}), and the blue ellipse the best fit ellip-

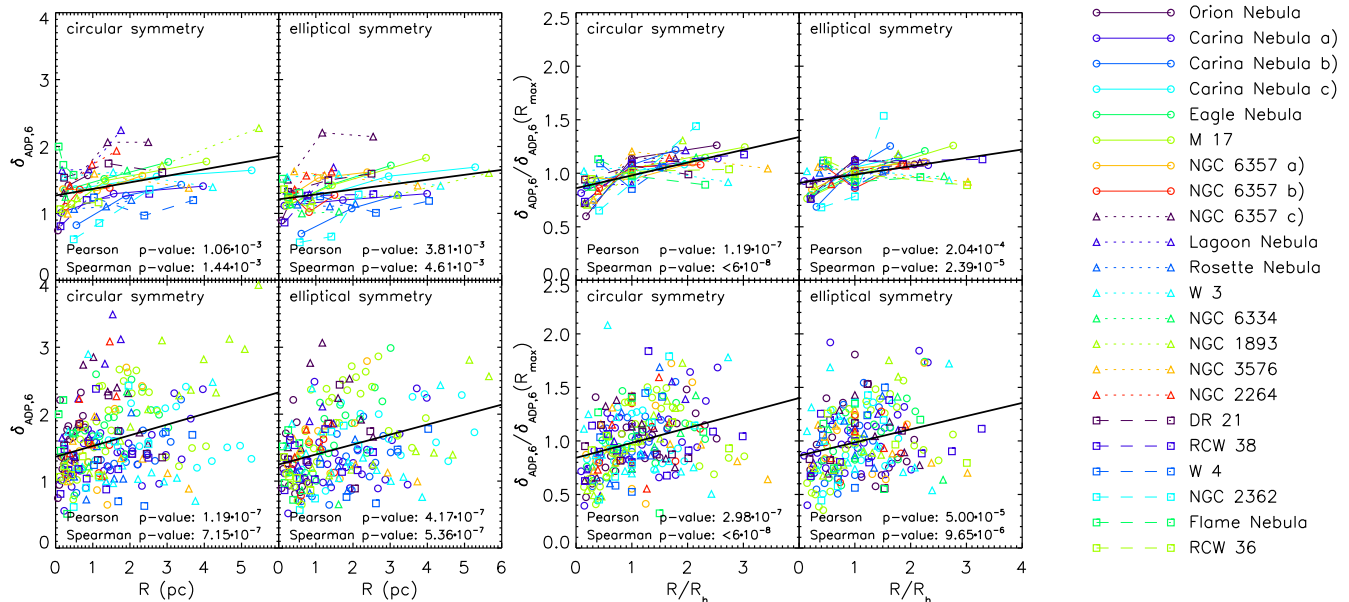


FIG. 3.— $\delta_{\text{ADP},6}$ vs R for all MYStIX regions of our analysis. Top panels indicate our low-resolution profiles (the average within 3 bins per cluster: R_{60} , R_h and R_{max}), bottom panels indicate the high-resolution profiles, where for each cluster all the radial bins from the center (each containing 60 sources) are denoted. The right-hand panels show the correlations between the quantities in each axis is normalized as indicated. The thick black line is the best fit to the data, and the correlation p -value is reported in each panel.

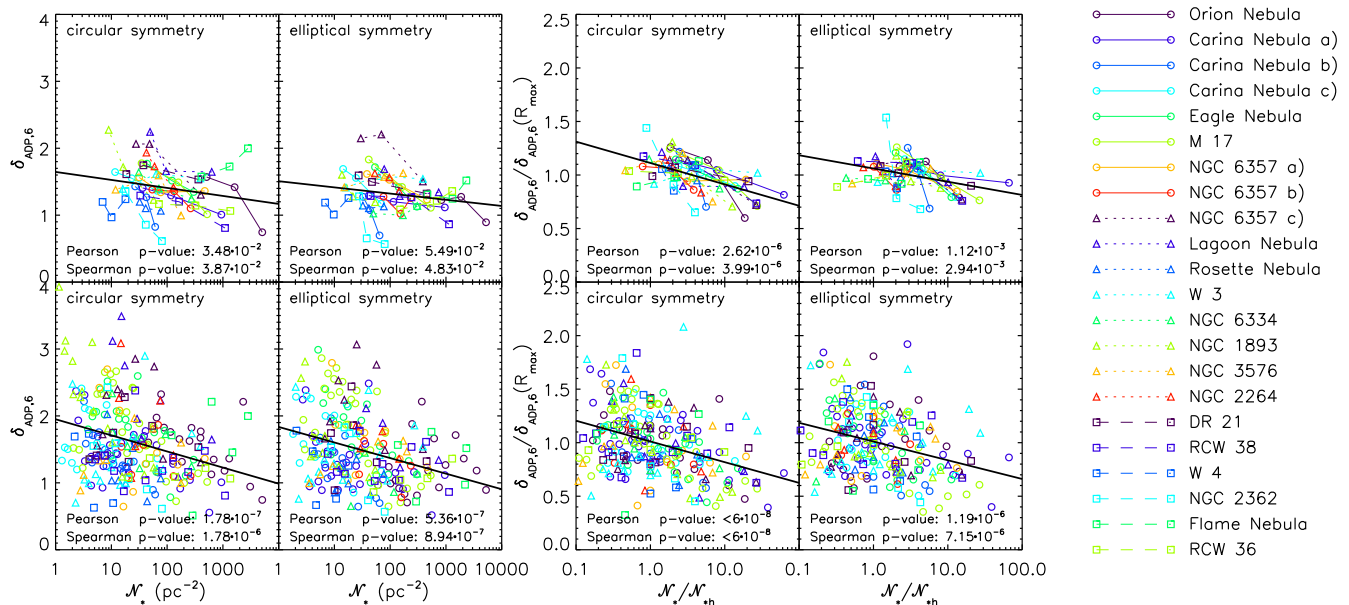


FIG. 4.— Same as Figure 3, for the correlation of $\delta_{\text{ADP},6}$ with surface density of stars \mathcal{N}_* .

tical model inside each of them.

We measure the radial profile of $\delta_{\text{ADP},6}$ for our identified MYStIX subclusters. Given the intrinsic difference in their number of members (from ~ 300 to ~ 1800 members, see Table 1), we adopt two choices: a) the *high resolution* profile, in which for both circular and elliptical symmetry we divide the populations in all concentric annuli containing 60 stars within R_{max} , and b) the *low resolution* profile, where we consider 3 radii: 1) R_{60} , i.e., the smallest circle from each center containing 60 stars; 2) the mean of $\delta_{\text{ADP},6}$ within the half-mass radius R_h ; 3) the mean of $\delta_{\text{ADP},6}$ within the cluster radius R_{max} . Since the MYStIX fields of view are not uniform, and because of our constraints (§2) to avoid overlapping of subclus-

ters in regions with multiple central concentrations, both R_{max} and R_h retain some arbitrariness. Also, the MYStIX cluster sample is heterogenous in that individual regions, depending on their distance and dust extinction, have different levels of (in)completeness. As we show in §4, such limitations are insufficient to erase the general qualitative trends we detect.

4. RESULTS

In Table 1 we report for each cluster the three radial bins of our low resolution profile, together with the total number of stars, annuli, and the average $\langle \delta_{\text{ADP},6} \rangle$ within R_{max} , all assuming circular symmetry. In nearly all cases $\delta_{\text{ADP},6} > 1$, indicating that none of these regions has

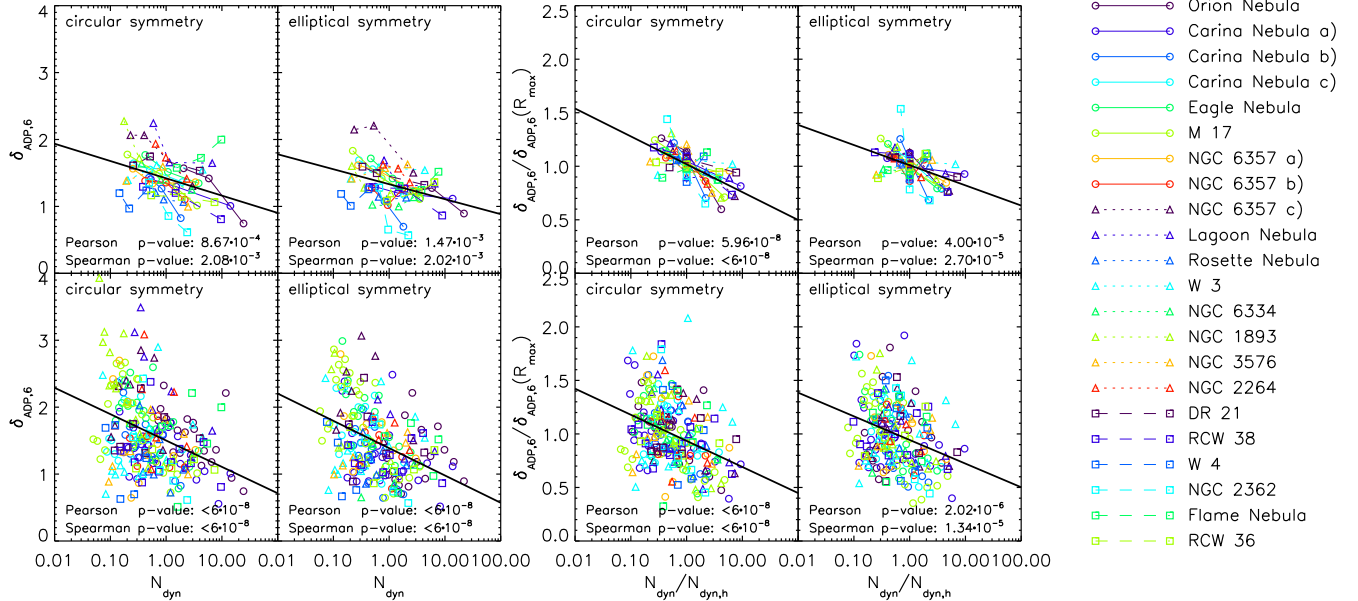


FIG. 5.— Same as Figure 4, for the correlation of $\delta_{\text{ADP},6}$ with dynamical age.

reached an isotropic spatial distribution of sources. In some cases (e.g., the clustered concentration of members in the Rosetta nebula), the value is fairly small; in others (e.g., NGC1893) $\delta_{\text{ADP},6}$ traces the visibly irregular spatial distribution of sources.

We look for systematic correlations in the degree of substructure with distance from the center and with surface density, employing the Pearson product-moment correlation coefficient and the Spearman correlation rank statistics. Specifically, we would expect that the core of the clusters, where the density is higher, would have reached a smoother distribution due to a higher rate of stellar interactions (scaling as the dynamical time or the free-fall time, $t_{\text{ff}} \propto \rho^{-1/2}$). In Table 1 we also report the one-sided p -values corresponding to a chance probability that either a positive trend of $\delta_{\text{ADP},6}$ versus R , or a negative trend of $\delta_{\text{ADP},6}$ versus the surface density of stars per pc^2 , \mathcal{N}_* , adopting the high-resolution δ_{ADP} profile. Indeed, for the majority of the clusters we identify a correlation, in some cases very significant ($p < 1\%$).

We also analyze these correlations considering all regions at once. In Figures 3 and 4 we present the dependence of $\delta_{\text{ADP},6}$ respectively on R and $\log \mathcal{N}_*$, using both our low- and high-resolution profiles, for both the assumptions of circular and elliptical apertures. As indicated by the p -values, the correlations become more significant, due to the increased number statistics, in particular in the high resolution δ_{ADP} profiles. These trends become slightly weaker when elliptical symmetry is adopted; this is because, as found in the ONC in DTJ14, this assumption naturally removes the first order of anisotropy in the stellar distribution, i.e., the presence of an elongation in a particular direction.

In Table 1 we also show for comparison the MST \mathcal{Q} parameter, computed for each cluster within R_h and R_{max} . Unlike for $\delta_{\text{ADP},N}$, where significant variations are measured within each cluster and among different clusters, all \mathcal{Q} values cluster around 0.8, the value generally assumed to discriminate between clumpy ($\mathcal{Q} < 0.8$) and centrally concentrated ($\mathcal{Q} > 0.8$) stellar distributions

(Cartwright & Whitworth 2004). This confirms that the \mathcal{Q} parameter is adequate to separate highly substructured regions, where individual clumps are evident, but has little or no diagnostic power for probing more moderate degrees of substructure within centrally-concentrated clusters, where $\delta_{\text{ADP},N}$ is far more sensitive¹. Also, interestingly, in most of our clusters \mathcal{Q} tends to be slightly larger at R_{max} than at R_h , indicating an opposite trend at that we detect from $\delta_{\text{ADP},N}$.

Considering the heterogeneity of the regions included in this analysis, both in terms of completeness (§3) and because each region may differ in their physical and dynamical age, we also test these correlations normalizing each quantity on some characteristic value typical of each cluster. Specifically, we consider δ'_{ADP} , which is δ_{ADP} normalized on its average for each particular cluster; also, the radius R' is R/R_h and the surface density $\mathcal{N}'_* = \mathcal{N}_*(R)/\mathcal{N}_*(R_h)$. The result is shown on the right-hand panels of Figures 3 and 4. Such normalizations always tighten the correlations, especially in the low-resolution case. We also tested if this improvement is particularly due to the normalization on one specific axis, considering all the combinations of such normalization. We found that for the $\delta'_{\text{ADP}}(R')$ trend, the normalization on δ'_{ADP} is the dominant factor, indicating that the MYStIX clusters may have inherent differences in their overall degree of substructure. On the other hand, both normalizations in $\delta'_{\text{ADP}}(\log \mathcal{N}'_*)$ contribute to the significance of the correlation between these quantities, probably due to the effect of inconsistent completeness affecting the densities we measure. From the linear fits of the high-density profiles, assuming circular symmetry, we measure: $\delta'_{\text{ADP},6} = 0.84 + 0.14R/R_h$ and $\delta'_{\text{ADP},6} = 1.01 - 0.19 \log \mathcal{N}'_*/\mathcal{N}'_{*,h}$, which are quantitative relations that can be compared to simulations of the dynamical evolution of young clusters.

¹ For a smooth isotropic stellar distribution within a sphere, \mathcal{Q} increases with central concentration: $\mathcal{Q} \simeq 0.8$ for constant volume density $n \propto r^0$ within a sphere; $\mathcal{Q} \simeq 0.95$ for $n \propto r^{-2}$

TABLE 1

Cluster	d	t_*	R_{60}	R_h	R_{\max}	n_{tot}	N_a	$\langle \delta_{\text{ADP},6} \rangle$			MST \mathcal{Q}	
	(pc)	(Myr)	(pc)	(pc)	(pc)			R_{60}	R_h	R_{\max}	R_h	R_{\max}
Orion Nebula	414	1.6	0.06	0.34	0.86	1200	20	0.74	1.42	1.57	0.83	0.89
Carina Nebula a)	2300	3.3	0.14	1.56	3.97	1800	30	1.01	1.30	1.41	0.79	0.90
Carina Nebula b)	2300	3.3	0.56	1.89	3.38	960	16	0.82	1.27	1.43	0.76	0.82
Carina Nebula c)	2300	3.3	0.54	2.72	5.27	1020	17	1.36	1.55	1.64	0.74	0.83
Eagle Nebula	1750	2.1	0.25	1.31	3.03	1260	21	1.35	1.52	1.77	0.79	0.90
M 17	2000	1.3	0.19	1.34	4.06	1800	30	1.01	1.49	1.78	0.81	0.99
NGC 6357 a)	1700	1.3	0.20	1.11	2.33	540	9	1.36	1.34	1.56	0.83	0.88
NGC 6357 b)	1700	1.3	0.27	0.65	1.45	360	6	1.10	1.36	1.38	0.80	0.89
NGC 6357 c)	1700	1.3	0.22	1.40	2.49	540	9	1.30	2.06	2.06	0.89	0.84
Lagoon Nebula	1300	2.1	0.17	0.89	1.76	480	8	1.65	1.66	2.24	0.86	0.84
Rosette Nebula	1330	3.1	0.50	1.36	2.04	420	7	1.07	1.10	1.20	0.80	0.80
W 3	2040	...	0.22	1.55	4.23	900	15	1.55	1.61	1.39	0.86	0.92
NGC 6334	1700	1.7	0.26	0.89	1.92	360	6	1.25	1.40	1.64	0.82	0.76
NGC 1893	3600	2.6	0.58	2.86	5.47	840	14	1.23	1.72	2.27	0.81	0.79
NGC 3576	2800	...	0.33	1.04	3.58	480	8	1.00	1.59	1.38	0.82	0.86
NGC 2264	913	2.4	0.38	0.98	1.64	360	6	1.41	1.73	1.93	0.78	0.76
DR 21	1500	1.9	0.23	1.43	2.87	480	8	1.53	1.74	1.61	0.80	0.80
RCW 38	1700	...	0.13	0.84	2.52	660	11	0.81	1.20	1.29	0.89	0.95
W 4	2040	...	1.03	2.39	3.70	300	5	1.24	0.97	1.20	0.81	0.85
NGC 2362	1480	3.5	0.49	1.18	2.53	360	6	0.61	0.86	1.36	0.81	0.87
Flame Nebula	414	1.0	0.08	0.21	0.48	300	5	2.00	1.73	1.58	0.74	0.93
RCW 36	700	1.3	0.12	0.42	1.16	300	5	1.06	1.14	1.16	0.88	0.99

Cluster	$\delta'_{\text{ADP}} =$									$N_{\text{dyn}} = t_*/t_{\text{dyn}}$		
	$a + b(\frac{R}{R_h})$			$a + b \log(\frac{N_*}{N_{*h}})$			$a + b \log(\frac{N_{\text{dyn}}}{N_{\text{dyn},h}})$					
	p -value	a	b	p -value	a	b	p -value	a	b	R_{60}	R_h	R_{\max}
Orion Nebula	0.009	0.77	0.19	0.007	1.02	-0.24	0.006	0.89	-0.32	24.4	5.84	2.06
Carina Nebula a)	0.002	0.76	0.22	0.002	1.02	-0.22	0.002	0.90	-0.29	14.2	1.52	0.53
Carina Nebula b)	0.003	0.59	0.39	0.002	1.00	-0.44	0.003	0.84	-0.57	1.83	0.83	0.49
Carina Nebula c)	0.509	1.00	-0.01	0.316	1.00	-0.06	0.309	0.98	-0.08	1.95	0.51	0.26
Eagle Nebula	0.005	0.73	0.25	0.002	1.02	-0.31	0.002	0.86	-0.41	3.83	1.08	0.42
M 17	0.051	0.85	0.13	0.003	1.01	-0.26	0.003	0.85	-0.35	3.60	0.75	0.20
NGC 6357 a)	0.039	0.55	0.44	0.088	1.05	-0.34	0.092	0.94	-0.43	3.35	0.57	0.25
NGC 6357 b)	0.273	0.88	0.09	0.214	0.98	-0.18	0.209	0.95	-0.23	2.16	0.99	0.42
NGC 6357 c)	0.450	0.98	0.02	0.233	1.03	-0.13	0.213	0.98	-0.17	2.96	0.40	0.23
Lagoon Nebula	0.012	0.46	0.50	0.025	1.06	-0.45	0.024	0.93	-0.58	6.70	1.15	0.59
Rosette Nebula	0.100	0.55	0.47	0.116	1.03	-0.50	0.121	0.93	-0.60	2.04	0.91	0.65
W 3	0.713	1.10	-0.08	0.806	0.99	0.14	0.814	1.05	0.18	4.50	0.68	0.21
NGC 6334	0.050	0.69	0.26	0.089	1.01	-0.27	0.079	0.95	-0.35	2.90	0.81	0.36
NGC 1893	0.001	0.35	0.62	0.001	1.03	-0.62	0.001	0.82	-0.79	1.37	0.33	0.18
NGC 3576	0.933	1.21	-0.13	0.843	1.02	0.15	0.842	1.06	0.19	2.47	0.87	0.19
NGC 2264	0.175	0.65	0.32	0.194	1.03	-0.37	0.192	0.94	-0.46	2.34	0.99	0.65
DR 21	0.805	1.12	-0.11	0.708	1.00	0.07	0.696	1.01	0.08	4.01	0.52	0.26
RCW 38	0.324	0.94	0.05	0.246	1.01	-0.09	0.240	0.97	-0.12	9.63	1.48	0.38
W 4	0.132	0.44	0.57	0.165	1.06	-0.59	0.173	0.94	-0.72	0.44	0.22	0.15
NGC 2362	0.040	0.29	0.58	0.037	0.96	-0.83	0.035	0.79	-1.07	2.39	1.10	0.49
Flame Nebula	0.722	1.19	-0.16	0.755	1.00	0.26	0.755	1.06	0.35	9.79	4.22	1.55
RCW 36	0.423	0.99	0.01	0.313	1.00	-0.04	0.310	0.99	-0.05	7.38	1.90	0.54

NOTE. — n_{tot} is the total number of stars within R_{\max} , dividend in N_a annuli. The Pearson's correlation coefficient p -values for each cluster are assuming the high resolution profile of $\delta_{\text{ADP},6}$ and circular symmetry. Values < 0.5 (green) indicate correlation in the expected direction. Cluster ages t_* are from Getman et al. (2014a). The dynamical ages N_{dyn} are lower limits (see text).

Last, changing the numbers of sectors to 4 or 9 does not affect these trends. Solely, as observed by DTJ14, increasing the number of sectors tends to decrease δ_{ADP} , indicating that the substructure of young stellar clusters is dominated by anisotropy on larger angular scales.

We also looked for trends of $\delta_{\text{ADP},N}$ with the median cluster age from Getman et al. (2014b), derived from the comparison of X-ray-derived stellar masses and extinction corrected J -band magnitudes for a sample of sources in each region. We detected no significant correlation for any choice of $\delta_{\text{ADP},N}$ for each cluster. This may be due to the fact that the cluster ages differ by up to a factor of 3 - compared to a much larger range of *dynamical* ages as a function of distance from the center within each cluster - and are in general very uncertain (e.g., Da Rio et al. 2010; Soderblom et al. 2013).

These results are amongst the first to probe dynamical evolution during and shortly after star cluster formation, specifically the dissolution of substructure in embedded systems with membership based on X-ray emission. Compared to other observational studies (Gutermuth et al. 2005, 2008; Ascenso et al. 2007; Schmeja et al. 2008; Getman et al. 2014a; Beccari et al. 2014), which have been able to qualitatively detect systematic differences in the location of younger and older stars in young clusters, and their morphology as a function of age, our results illustrate how $\delta_{\text{ADP},N}$ can be a metric of relative local dynamical age, which is greater in central, denser regions.

For gravitationally bound, virialized systems with virial parameter $\alpha_{\text{vir}} \equiv 5\sigma^2 R/(GM)$, where σ is the 1D mass-averaged velocity dispersion, we can assess the dy-

namical age t_*/t_{dyn} . Here t_* is the actual age of the system and $t_{\text{dyn}} \equiv R/\sigma$ is the local dynamical time. Thus

$$\frac{t_*}{t_{\text{dyn}}} = 1.06\alpha_{\text{vir}}^{1/2} \left(\frac{t_*}{2 \text{ Myr}} \right) \left(\frac{\Sigma}{100 M_{\odot} \text{ pc}^{-2}} \right)^{1/2} \left(\frac{R}{\text{pc}} \right)^{-1/2}, \quad (2)$$

where $\Sigma \equiv M/(\pi R^2)$. The conversion between \mathcal{N}_* and Σ depends on the mean stellar mass of the X-ray-detected sources, the degree of incompleteness of the stellar population and the contributions of gas. For a near complete stellar census and a similar mass of gas and stars we expect $\Sigma \simeq (\mathcal{N}_*/\text{pc}^{-2})M_{\odot} \text{ pc}^{-2}$. With the exception of the ONC, most of the MYStIX clusters are expected to be more incomplete in their stellar census, due to their farther distances, and lower Chandra exposure times in X-rays. As described in Feigelson et al. (2013), however, the characterization of the completeness in each MYStIX region is challenging because the membership assignment from Broos et al. (2013) is quite restrictive and the completeness depends also on IR data and the reddening and crowding on each region.

Still, using this conversion factor we may derive a lower limit on the dynamical age at R_{60} , R_h and R_{max} . We have adopted the median age for each region from Getman et al. (2014a), which is available for all except four of our subclusters, which have been assigned a typical age of 2 Myr. We have also adopted $\alpha_{\text{vir}} = 1$ as a fiducial value.

Values $N_{\text{dyn}} = t_*/t_{\text{dyn}} \gtrsim 1$ then indicate this region of the cluster is older than a crossing time, and thus likely to be gravitationally bound and subject to dynamical smoothing of substructure. As reported in Table 1, all our clusters appear older than 1 t_{dyn} at least in the core region (R_{60}), and in some cases up to R_h . This conclusion is reinforced considering that our estimates of N_{dyn} are lower limits due to incompleteness.

Figure 5 shows the profiles of $\delta_{\text{ADP},N}$ as a function of N_{dyn} ; we find that δ_{adp} decreases with increasing dynamical age, and reaches values close to unity after a few dynamical times (although values of N_{dyn} here are likely lower limits). Despite the uncertainties in α_{vir} and Σ for each cluster, the correlation p-values in Figure 5 are always smaller than those derived for $\delta_{\text{ADP},N}$ as a function of R and \mathcal{N}_* , indicating a tighter fit. As for the other parameters, Table 1 also reports the best fit simple function correlation results for each individual cluster, showing a behavior similar to that of $\delta_{\text{ADP},N}$ versus \mathcal{N}_* .

Measuring the degree of substructure was proposed as a way to assess whether star cluster formation was dynamically slow or rapid (Tan et al. 2006). We expect the quantitative dependence of $\delta_{\text{ADP},N}(R, \mathcal{N}_*, t/t_{\text{dyn}})$ is an important constraint against which to test theoretical models of star cluster formation.

As we have shown, $\delta_{\text{ADP},N}$ constitutes a much more sensitive estimator of substructure within centrally concentrated clusters or subclusters than the MST Q parameter, and advocate its use in both observational and theoretical studies of early cluster evolution.

The absolute ages and age spreads of young star clusters are very difficult to measure and current estimates contain significant uncertainties. Still, the results of future studies assessing such ages and age spreads of these star clusters systematically can be compared with our $\delta_{\text{ADP},N}(R, \mathcal{N}_*, t/t_{\text{dyn}})$ results to place the discovered structural evolution on an absolute timescale.

KOJ and JCT acknowledge support from NASA Astrophysics Theory and Fundamental Physics grant ATP09-0094. NDR acknowledges support from the Theory Postdoctoral Fellowship from the University of Florida Department of Astronomy and College of Liberal Arts and Sciences.

REFERENCES

- Allison, R. J., Goodwin, S. P., Parker, R. J., et al. 2009, *ApJ*, 700, L99
- André, P., Di Francesco, J., Ward-Thompson, D., et al. 2013, [arXiv:1312.6232](https://arxiv.org/abs/1312.6232)
- Ascenso, J., Alves, J., Vicente, S., & Lago, M. T. V. T. 2007, *A&A*, 476, 199
- Bastian, N., Gieles, M., Ercolano, B., & Gutermuth, R. 2009, *MNRAS*, 392, 868
- Beccari, G., DeMarchi, G., Panagia, N., et al. 2014, *A&A*, *in press* ([arXiv:1409.4370](https://arxiv.org/abs/1409.4370))
- Broos, P. S., Getman, K. V., Povich, M. S., et al. 2013, *ApJS*, 209, 32
- Cartwright, A., & Whitworth, A. P. 2004, *MNRAS*, 348, 589
- Da Rio, N., Tan, J. C., Jaehnig, K. O. 2014, *ApJ*, 795, 55
- Da Rio, N., Gouliermis, D. A., & Gennaro, M. 2010, *ApJ*, 723, 166
- Feigelson, E. D., Townsley, L. K., Broos, P. S., et al. 2013, *ApJS*, 209, 26
- Fellhauer, M., Wilkinson, M. I., & Kroupa, P. 2009, *MNRAS*, 397, 954
- Getman, K. V., Feigelson, E. D., Kuhn, M. A., et al. 2014, *ApJ*, 787, 108
- Getman, K. V., Feigelson, E. D., & Kuhn, M. A. 2014, *ApJ*, 787, 109
- Goodwin, S. P., & Whitworth, A. P. 2004, *A&A*, 413, 929
- Gutermuth, R. A., Megeath, S. T., Pipher, J. L., et al. 2005, *ApJ*, 632, 397
- Gutermuth, R. A., Myers, P. C., Megeath, S. T., et al. 2008, *ApJ*, 674, 336
- Gutermuth, R. A., Megeath, S. T., Myers, P. C., et al. 2009, *ApJS*, 184, 18
- Kirk, H., Johnstone, D., & Tafalla, M. 2007, *ApJ*, 668, 1042
- Kruijssen, J. M. D., Maschberger, T., Moeckel, N., et al. 2012, *MNRAS*, 419, 841
- Kuhn, M. A., Feigelson, E. D., Getman, K. V., et al. 2014, *ApJ*, 787, 107
- Lada, C. J., & Lada, E. A. 2003, *ARA&A*, 41, 57
- Maschberger, T., Clarke, C. J., Bonnell, I. A., & Kroupa, P. 2010, *MNRAS*, 404, 1061
- Parker, R. J. 2014, [arXiv:1410.0004](https://arxiv.org/abs/1410.0004)
- Parker, R. J., Wright, N. J., Goodwin, S. P., & Meyer, M. R. 2014, *MNRAS*, 438, 620
- Parker, R. J., & Meyer, M. R. 2012, *MNRAS*, 427, 637
- Proszkow, E.-M., & Adams, F. C. 2009, *ApJS*, 185, 486
- Scally, A., & Clarke, C. 2002, *MNRAS*, 334, 156
- Schmeja, S., Kumar, M. S. N., & Ferreira, B. 2008, *MNRAS*, 389, 1209
- Schmeja, S., & Klessen, R. S. 2006, *A&A*, 449, 151
- Soderblom, D. R., Hillenbrand, L. A., Jeffries, R. D., Mamajek, E. E., & Naylor, T. 2013, [arXiv:1311.7024](https://arxiv.org/abs/1311.7024)
- Tan, J. C., Krumholz, M. R., & McKee, C. F. 2006, *ApJ*, 641, L121